

ATMOSPHERE, INTERIOR, AND EVOLUTION OF THE METAL-RICH TRANSITING PLANET HD 149026B

J. J. FORTNEY¹, D. SAUMON², M. S. MARLEY¹, K. LODDERS³, R. S. FREEDMAN^{1,4}
Submitted to ApJ, July 15, 2005

ABSTRACT

We investigate the atmosphere and interior of the new transiting planet HD 149026b, which appears to be very rich in heavy elements. We first compute model atmospheres at metallicities ranging from solar to ten times solar, and show how for cases with high metallicity or inefficient redistribution of energy from the day side, the planet can develop a hot stratosphere due to absorption of stellar flux by TiO and VO. The resulting spectra of these models are very different than cooler atmosphere models without stratospheres. The spectral effects are potentially detectable with the *Spitzer Space Telescope*. In addition the models with hot stratospheres lead to a large limb brightening, rather than darkening. Using a grid of self-consistent model atmospheres and high-pressure equations of state for all components, we compute thermal evolution models of the planet, and estimate that the mass of heavy elements within the planet is in the range of 66 to 79 M_{\oplus} . Finally, we discuss trends in the radii of transiting planets with metallicity in light of this new member of the class.

Subject headings: planetary systems, radiative transfer, binaries:eclipsing, stars: individual (HD 149026)

1. INTRODUCTION

Searches for extrasolar giant planets (EGPs) over the past ten years have yielded a bizarre menagerie of planets, many of which are in orbits with periods of only a few days. These “hot Jupiters,” or “Pegasi planets,” which orbit within ~ 0.1 AU of their parent stars, form a class of astrophysical objects that is still yielding surprises. The latest, and perhaps most unanticipated, is HD 149026b, a planet in a 2.87 day orbit around a metal-rich G0 IV parent star. This planet was discovered by the radial velocity method and subsequently shown to transit its parent star (Sato et al. 2005). The most striking feature of planet HD 149026b is its small radius of only $0.725 \pm 0.05 R_J$, given its mass of $0.36 \pm 0.03 M_J$ ($114 M_{\oplus}$). For comparison, Saturn has a mass of $0.30 M_J$ ($95 M_{\oplus}$), is about 2.5 Gyr older than HD 149026b and receives 140,000 times less stellar flux, and yet has a mean radius of $0.81 R_J$. The transiting planet most similar in mass to HD 149026b, OGLE-Tr-111b, has a mass of $0.53 M_J$ and a radius of $\sim 1 R_J$ (Pont et al. 2004).

Evolution models of Pegasi planets have shown that lower-mass giant planets should be preferentially influenced by irradiation, leading to larger radii (Guillot et al. 1996), but HD 149026b is decidedly small. Recent interior structure models of Saturn show that it globally possesses $20 \pm 8 M_{\oplus}$ of heavy elements (including the core) for a corresponding global enhancement in “metals” of 6–14 fold relative to the Sun (Saumon & Guillot 2004). The small radius of HD 149026b implies that it has even more heavy elements in its interior. Indeed Sato et al. (2005) have estimated a core mass near $70 M_{\oplus}$, or 60% of the planet’s mass! The high metallicity of the parent star $[\text{Fe}/\text{H}] = 0.36 \pm 0.05$ (Sato et al. 2005) suggests that this system is very favorable to planet formation as the current

fraction of stars with detected planets increases strongly with stellar metallicity (Gonzalez 1997; Santos et al. 2004; Fischer & Valenti 2005).

While the planet’s orbital radius of 0.042 AU is similar to that of the well-known transiting planet HD 209458b, the luminosity of the star HD 149026 is larger ($2.7 L_{\odot}$), and the degree of irradiation is intermediate between those of well known transiting planets OGLE-Tr-56b ($T_{\text{eff}} \sim 1950$ K) and HD 209458b ($T_{\text{eff}} \sim 1450$ K). We will show that the atmosphere of HD 149026b could be substantially different from that of HD 209458b and TrES-1, which were recently detected in the infrared with the *Spitzer Space Telescope* (Deming et al. 2005; Charbonneau et al. 2005). As the HD 149026 system is relatively bright ($V = 8.15$) it is an enticing target for follow up *Spitzer* observations.

In this paper we investigate atmosphere models for the planet and show how under certain circumstances the atmosphere features a hot stratosphere driven by absorption of stellar flux by TiO and VO at mbar pressures. We provide model planet-to-star flux density ratios in *Spitzer* IRAC and MIPS bandpasses that will allow for a determination of the character of the planet’s atmosphere. We also investigate the evolutionary history of HD 149026b with the help of a new grid of model atmospheres computed specifically for this planet. This atmosphere grid, applied to a planetary evolution code, with high-pressure equations of state of H/He mixtures, rock and ice, allow us to place constraints on the abundances of heavy elements in HD 149026b, and to begin to understand its current structure.

¹ Space Science and Astrobiology Division, NASA Ames Research Center, MS 245-3, Moffett Field, CA 94035; jfortney@arc.nasa.gov

² Los Alamos National Laboratory, MS F699, Los Alamos, NM 87545

³ Planetary Chemistry Laboratory, Department of Earth and Planetary Sciences, Washington University, St. Louis, MO 63130

⁴ SETI Institute, 515 N. Whisman Road, Mountain View, CA 94043

2. MODEL ATMOSPHERES

2.1. Methods

Atmospheric pressure-temperature (P - T) profiles and spectra for the planet were obtained with a plane-parallel model atmosphere code that has been used for a variety of planetary and substellar objects. The code was first used to generate profiles and spectra for Titan’s atmosphere by McKay et al. (1989). It was significantly revised to model the atmospheres of brown dwarfs (Marley et al. 1996; Burrows et al. 1997; Marley et al. 2002), Uranus (Marley & McKay 1999), cool EGPs (Marley 1998), and Pegasi planets (Fortney et al. 2005). It explicitly includes both incident radiation from the parent star and thermal radiation from the planet’s atmosphere and interior. The basic radiative transfer solving scheme was developed by Toon et al. (1989). We use the elemental abundance data of Lodders (2003) and compute chemical equilibrium compositions with the CONDOR code, following Fegley & Lodders (1994) and Lodders & Fegley (2002).

In addition we maintain a large and constantly updated opacity database. Our dataset includes the molecular lines of H_2O , CH_4 , CO , NH_3 , H_2S , PH_3 , TiO , VO , CrH , FeH , CO_2 , HCN , and C_2H_2 complemented with the atomic lines of the alkali metals (Li, Na, K, Rb and Cs) from Burrows et al. (2000) and continuum opacity sources from H_2 CIA, H_2 , H and He Rayleigh scattering, and H^- bound-free and free-free, H_2^- free-free, He^- free-free, and H_2^+ bound-free and free-free (Freedman & Lodders, in prep.).

We predict all cloud properties using the model of Ackerman & Marley (2001), which is directly coupled to the radiative transfer solver. The model parameterizes the efficiency of sedimentation of cloud particles through an efficiency factor, f_{sed} . Large values of f_{sed} correspond to rapid particle growth and large mean particle sizes. In this case condensates quickly fall out of the atmosphere, leading to physically and optically thin clouds. When f_{sed} is small, cloud particles grow more slowly and the atmospheric condensate load is larger and the clouds are both physically and optically thicker. Here we use a sedimentation efficiency parameter $f_{\text{sed}} = 3$, which fits spectral observations of cloudy L-dwarfs (Marley et al. 2002). This choice generally places 90% of the optical depth of a cloud within 1 scale height of the cloud base. While a large number of condensates are included in the calculation of the chemical equilibrium, the cloud model here accounts for the major condensible species Fe and Mg-silicates (here represented by Mg_2SiO_4). Further details on our methods can be found in Marley et al. (2002) and Marley et al. (in prep.).

We model the impinging stellar flux from 0.26 to 10.0 μm and the emitted thermal flux from 0.26 to 325 μm . All the relevant planetary and stellar parameters for HD 149026b are taken from Sato et al. (2005). The incident stellar flux from HD 149026 is from a model spectrum by Kurucz (1993) with a $T_{\text{eff}} = 6200$ K model interpolated in gravity to $\log g = 4.26$. The luminosity of the final stellar model matches the Sato et al. (2005) derivation of $2.7 L_{\odot}$. The planet’s radiative-convective P - T profile is arrived at iteratively until the net flux is conserved to at least one part in 10^6 in each layer. Our model atmosphere code computes the P - T profile and a low resolution spec-

trum. A high-resolution spectrum is generated from the P - T profile and a full line-by-line radiative transfer code, using the same chemistry, opacity database and converged cloud properties.

When modeling the atmospheres of irradiated objects with a one-dimensional, plane parallel atmosphere code it is necessary to weight the stellar flux F by a geometric factor that is the ratio of the cross-section area of the planet to the surface area of the emitting planetary surface. If the planet is able to reradiate the absorbed stellar energy over its entire surface (4π steradians), an incident stellar flux of $F/4$ is used. This assumes a very efficient horizontal redistribution of the absorbed stellar energy over the entire atmosphere. In the other limit, redistribution is poor and the planet is only able to reradiate this flux on the day side (2π steradians) and the normalization is $F/2$. Here our standard case is $F/4$. All models shown will use $F/4$ unless they are labeled “ 2π ,” in which case $F/2$ is used. Models of the atmospheres of TrES-1 and HD 209458b are in better agreement with the *Spitzer* observations (Charbonneau et al. 2005; Deming et al. 2005) when efficient redistribution ($F/4$) is assumed (Fortney et al. 2005; Seager et al. 2005; Barman et al. 2005). This conclusion is tentative however, and Burrows et al. (2005) argue for a value between $F/4$ and $F/2$. An intermediate value (although closer to $F/4$) is supported by the most recent dynamical models for HD 209458b (Cooper & Showman 2005) that predict a temperature contrast between the “hot” and “cold” sides of the planet of ~ 500 K, which may be blown by supersonic winds 60 degrees from the planet’s day and night sides.

2.2. Spectra, Composition, & Energy Balance

We have computed atmospheric P - T profiles for three metallicities: $[\text{M}/\text{H}] = 0, 0.5, \text{ and } 1$. These profiles are shown in Fig. 1. The solar metallicity model allows a comparison with published models of the planets HD 209458b and TrES-1, the $[\text{M}/\text{H}] = 0.5$ is close to the metallicity of the star HD 149026, and $[\text{M}/\text{H}] = 1$ represents an enrichment of ~ 3 times over the star’s value, which is typical of the atmospheres of Jupiter and Saturn. These atmosphere models assume 1) reradiation of the absorbed stellar flux over 4π steradians, 2) cloudless structures, and 3) an intrinsic temperature (the T_{eff} the planet would have in isolation) of 100 K, which we will later show to be realistic, based on thermal evolution models (§3.1). As the metallicity is increased, the atmosphere becomes warmer as a larger fraction of incident radiation is absorbed. These profiles all exhibit hot stratospheres due to absorption by TiO and VO at mbar pressures. However, the P - T profiles all cross the condensation curve of CaTiO_3 at pressures of hundreds of bars (marginally so for the $[\text{M}/\text{H}] = 1$ model however). Due to mixing in the atmosphere, all gaseous TiO in the upper atmosphere would eventually mix down to this condensation point, where the CaTiO_3 cloud remains confined, due to the gravitation field. This process, known as a “cold trap,” is responsible for the extremely low water abundance in the Earth’s stratosphere. Based on the profiles shown in Fig. 1, there should be no gaseous TiO at low pressures. This effect was pointed out for irradiated planetary atmospheres by Hubeny et al. (2003), and we obtain qualitatively similar results. The cold trap phe-

nomenon constitutes a departure from chemical equilibrium that cannot be accounted for in pre-tabulated chemical equilibrium abundances. To simplify our calculations, we use the CaTiO_3 condensation curve as the boundary to determine the availability of gaseous TiO and VO, although VO is less refractory than TiO. Given other uncertainties, and that TiO is 10 times more abundant than VO, this is a reasonable approximation. A thorough description of Ti and V chemistry in substellar atmospheres is given in Lodders (2002).

Because we do not include the TiO and VO cold trap, the $[\text{M}/\text{H}]=0$ and 0.5 profiles in Figure 1 are merely illustrative. Since TiO and VO should not be present at low pressures, we now remove their opacity from the calculation at pressures below 10 bar. These revised profiles are shown in Figure 2, and also include the opacity of Mg-silicates (here as forsterite, Mg_2SiO_4) and iron (Fe) clouds. These cloudy profiles are slightly warmer at low pressures than cloudless profiles would be. Both models absorb nearly all incident stellar flux, with only 8% and 5% of this flux being reflected back to space, for $[\text{M}/\text{H}]=0$ and 0.5 , respectively.⁵ The stellar flux is absorbed at progressively lower pressures as the metallicity is increased. We also show a $[\text{M}/\text{H}]=0.5$ model assuming reradiation over the day side only (2π steradians). This model is significantly hotter and does not cross the CaTiO_3 condensation curve. Therefore, TiO and VO will be present at low pressures, leading to a hot stratosphere. We also include the $[\text{M}/\text{H}]=1$ model from Figure 1 as a viable model, as a very slight increase in T_{int} (~ 10 K) would lead to a profile that does not reach this important condensation curve. All the models shown in Figure 2 are realistic profiles for the assumed metallicities. However, it is unlikely that the planet has a lower metallicity than the parent star ($[\text{Fe}/\text{H}]=0.36 \pm 0.05$, Sato et al. 2005). For the remainder of the discussion, we will consider only the $[\text{M}/\text{H}]=0.5$ and 1 models.

We also note that a cold trap will in general affect additional chemical species, but this is of minor importance for our profiles. Along with TiO and VO we also remove FeH and CrH at pressures below 10 bars, although these hydrides do not provide much opacity. Cold traps do have the potential to change the abundance of oxygen in the upper atmosphere. For instance, here we do no account for the 1% of available oxygen that corundum (Al_2O_3) cloud formation will remove in the upper atmosphere at pressures lower than 10 bars. Most importantly, one could envision a profile where silicates condensed at high pressure (here they do not), but then at lower pressures the temperature profiles could be warmer than the silicate condensation curves. If so, then our chemical equilibrium abundance tables would significantly overestimate the abundance of available oxygen. The Mg-silicates remove 23% of oxygen in a solar composition gas, which would increase the C/O ratio in the upper atmosphere. This would lead to a decrease in the mixing ratio of H_2O and an increase in the mixing ratio of CO as compared to the chemical equilibrium prediction (Fortney et al. 2005). Such concerns may be relevant to atmospheres encountered in the future.

The spectra of the $[\text{M}/\text{H}]=0.5$ and 1 models are plotted in Figure 3. Like other Pegasi planets, the infrared spec-

trum is carved by H_2O and CO opacity. We find no spectral signatures due to CH_4 as CO is by far the dominant carbon reservoir in these hot atmospheres. Interestingly, the stratosphere of the $[\text{M}/\text{H}]=1$ model results in *emission* features of H_2O and CO. For example, the series of spikes in the $4.2 - 5.5 \mu\text{m}$ spectral region are all CO emission features. Emission due to TiO and VO is also seen in the optical, whereas in the $[\text{M}/\text{H}]=0.5$ model the optical spectrum is carved by strong absorption by Na and K. We plot our planet-to-star flux density ratios in Figure 4 and show the wavelength ranges of the 4 IRAC bands and MIPS $24 \mu\text{m}$ band. The models with stratospheres are redder from 4 to $20 \mu\text{m}$ than models without stratospheres, due to emission by CO and H_2O , which can be seen most strongly in IRAC 4.5, 5.8, and $8.0 \mu\text{m}$ bands. Comparing photometry in these IRAC bands to the $3.6 \mu\text{m}$ band will be the most clear signature of a stratosphere for this planet, as well as other transiting planets.

Table 1 collects our band-averaged planet-to-star flux density ratios in the *Spitzer* IRAC and MIPS bands. Due to the combination of the planet’s small radius and the large luminosity of the parent star, these ratios are typically $\sim 1/4$ to $1/2$ of those for TrES-1, assuming “ 4π ” reradiation. Detection may be difficult. Deciding the best bands to search in will depend on the band-dependant photon-noise limited errors. Looking at IRAC specifically, while the planet is brightest at $8.0 \mu\text{m}$, the instrument is more sensitive in the shorter wavelength bands. As TrES-1 seems to be redder than expected in the infrared (Fortney et al. 2005; Barman et al. 2005) we encourage a comparison of photometry of all four IRAC bands for this planet (and HD 209458b) as that data becomes available.

2.3. Limb Darkening and Brightening

A diagnostic of the atmospheres of transiting planets is the variation in surface brightness of the planet’s disk which is in principle observable during the secondary eclipse ingress and egress. Limb darkening is particularly interesting as it provides an empirical determination of the temperature profile of the atmosphere at optical depths less than unity. We have computed the planet’s limb darkening over the *Spitzer* bandpasses. Depending on the atmosphere model, both limb brightening and darkening can occur. Particularly, we find that limb brightening is a sensitive diagnostic of stratospheric heating, with a strong signature in the $[\text{M}/\text{H}]=1$ model. Figure 5 plots the normalized specific intensity across the planetary disk for our cloudy $[\text{M}/\text{H}]=0.5$ and the cloudless $[\text{M}/\text{H}]=1$ models. We have used the transit code described in Hubbard et al. (2001) to compute ingress lightcurves for the limb brightened and darkened planets. Unfortunately the difference between these lightcurves is only $\sim 1\%$, so the effect is not detectable with *Spitzer*. We hold out hope for the *James Webb Space Telescope*, however. Therefore, for the foreseeable future, IRAC photometry remains the best method for determining the existence of Pegasi planet stratospheres.

3. EVOLUTION MODELS

3.1. Methods

⁵ These values are not necessarily equivalent to the Bond albedo, as we are using a plane parallel, one-dimensional model atmosphere code.

We have generated a grid of atmospheres for the purpose of modeling the evolution of HD 149026b. This is a grid of cloudless atmospheres with $[M/H]=0.5$, with TiO and VO removed at low pressure by the “cold trap” effect. The stellar flux is diluted by a factor of 1/4, as described in Section 2.1. As we predict that the silicate and iron clouds have a combined optical depth of ~ 0.1 , neglecting the clouds leads to a very slightly cooler P - T profile in the upper atmosphere but the structure of the deep atmosphere is essentially unchanged from the profile shown in Figure 2. We assume that the stellar luminosity is constant with time and that the planet was remained at 0.042 AU for all ages. We have calculated atmosphere models at 12 values of T_{int} and 3 gravities, that cover the parameters of planet HD 149026b for ages between $\sim 10^6$ to 5×10^9 years. Even at very young ages (< 10 Myr), when the planet has an appreciable internal energy source, the incident flux dominates the planet’s intrinsic flux, and T_{eff} is only 30 K higher than T_{eq} .

Our evolution code for the calculation of the cooling and contraction of adiabatic giant planets is well-tested. It has been used to produce evolutionary models of Jupiter and Saturn (Fortney & Hubbard 2003) and cool extrasolar giant planets (Fortney & Hubbard 2004) and it is described in detail in Fortney & Hubbard (2003). No modifications to the code were needed to calculate the evolution and contraction of Pegasi planets. The radiative atmosphere that serves as the bottleneck for cooling above the adiabatic H/He envelope is automatically accounted for with our fully non-gray, self-consistent model atmosphere grid. The importance of using detailed atmosphere models for evolutionary calculations of Pegasi planets is discussed in Baraffe et al. (2003).

For the equation of state (EOS) of the H/He envelope we use the Saumon et al. (1995) EOS with a helium mass fraction $Y = 0.27$. In order to include heavy elements accurately we use the ANEOS zero-temperature EOSs (Thompson 1990) of water (for generic ices, which is predominantly water) and olivine (for generic “rocks”). Zero-temperature EOSs are suitable for these constituents, as the thermal contribution to the pressure for ices in out density/temperature range is on the order of 10-20% (Hubbard & Macfarlane 1980) and is considerably lower for rock. Later we will show this has very little effect on our derived core size. The use of a zero-temperature EOS implies that we ignore the heat content of the core on the thermal history of the planet. This is often done for evolutionary models of Jupiter and Saturn (Hubbard 1977; Saumon et al. 1992; Fortney & Hubbard 2003), as the error involved is small compared to other unknowns, such as the temperature of the H/He envelope at Mbar pressures (Saumon & Guillot 2004) and the radiative properties of the planets’ atmospheres. At first glance, this may seem a gross simplification for HD 149026b, where the heavy elements may constitute 2/3 of the planet’s mass. However, as noted in Hubbard (1978) in regard to the cooling of Uranus and Neptune, the heat capacity of a species is inversely proportional to its molecular weight, meaning the heat content of the ices is ~ 0.1 that of H, and for rocks this ratio is only a few hundredths.

Modeling the heat content of the core would require a knowledge of the mechanism of energy transport within

the core. If energy were transported by convection, the temperature gradient would be close to an adiabat but if conduction is the dominant mechanism, the core could be close to isothermal. Furthermore, interior composition gradients can inhibit convection and result in steep super-adiabatic temperature gradients, as may be the case for Uranus and Neptune. Adiabatic models for Uranus and Neptune overestimate the current luminosity of both planets (Podolak et al. 1991), supporting such a possibility.

It should be remembered that compared to Jupiter and Saturn, relatively little is understood about the interiors of Uranus and Neptune. Our understanding of Jupiter and Saturn forms a solid basis for modeling the structure of extrasolar *gas* giants but the same cannot be said about extrasolar *ice* giants. (For an in-depth discussion of the structure and cooling history of the solar system’s ice giants, see the excellent reviews by Podolak et al. 1991 and Hubbard et al. 1995.) Given the considerable uncertainties in modeling the interior structure of a planet for which only the mass and radius are known, we believe the EOSs and treatment we have chosen here are quite acceptable.

We also neglect the “transit radius” effect: The apparent radius of a transiting planet is the radius where the slant optical depth through the planet’s atmosphere reaches unity. The corresponding atmospheric pressure can vary across many orders of magnitude, depending on the wavelength (Fortney et al. 2003). Burrows et al. (2003) and Baraffe et al. (2003) have estimated this effect to be $\sim 10\%$ and 5% respectively, for HD 209458b, compared to some reference radius, such as the radiative-convective boundary or the 1 bar level. However, the transit radius effect is considerably smaller for HD 149026b because of its higher gravity (1700 cm/s^2) and the broad photometric bandpasses use by Sato et al. (2005). Furthermore, the reported error on the radius of HD 149026b is $\pm 3.5\%$, larger than the expected transit radius effect.

In their discovery paper, Sato et al. (2005) used planet modeling techniques described in Bodenheimer et al. (2003) to model the contraction history and current structure of HD 149026b. They modeled the planet as a solar composition H/He envelope on top of a uniform density core of either 5.5 g cm^{-3} (for ices) or 10.5 g cm^{-3} (for rocks). They also implicitly ignore the heat content of the core. Constant density models ignore the actual high-pressure equation of state and are simplistic. However, as we will see, our estimates for the total heavy element abundances, using detailed non-gray atmosphere models and advanced equations of state for ice and rock essentially confirm the preliminary findings of Sato et al. (2005).

3.2. Internal Structure and Composition

We will take a straightforward look at possible interior models of HD 149026b. Since we have used $[M/H]=0.5$ for the model atmosphere grid, we also assume the H/He envelope down to the core is similarly enhanced in heavy elements. We use our ice EOS to mix in $Z=0.045$ into the pressure-density relation of the H/He envelope, using the additive volume rule,

$$\frac{1}{\rho} = \frac{1-Z}{\rho_{H/He}} + \frac{Z}{\rho_{\text{ice}}}. \quad (1)$$

We assume that the core is made either entirely of rock or ice. At the estimated age of 2 Gyr for HD 149026 (Sato

et al. 2005), we find that a core mass of $65.5 M_{\oplus}$ of rocks or of $77 M_{\oplus}$ of ices is consistent with the currently derived planetary radius. Including $\sim 2 M_{\oplus}$ of heavy elements in the envelope ($Z=0.045$), we derive a total mass of heavy elements for each model of 68 and $79 M_{\oplus}$. The contraction of the radius of the two planet models are shown in Figure 6.

As a check on these results, we also investigated the contraction of HD 149026b with an alternative “rock” and “ice” EOS, which are given in Hubbard & Marley (1989). These EOSs are polynomial fits to high pressure EOSs given in Zharkov & Trubitsyn (1978). “Rock” is a mixture of 38% SiO_2 , 25% MgO , 25% FeS , and 12% FeO . This material is slightly denser at high pressure than our ANEOS rock EOS, leading to a total heavy element mass in the planet of $66 M_{\oplus}$. “Ice” here is a mixture of 56.5% H_2O , 32.5% CH_4 , and 11% NH_3 at temperatures of $\sim 10^4$ K. We find a total heavy element mass of $78 M_{\oplus}$. Our conclusions regarding heavy elements remain essentially unchanged despite using a different composition for the rock and a non-zero temperature EOS for the ice mixture. The evolution models show that the interior of HD 149026b has cooled significantly, which is not surprising given the relatively small percentage of its mass contributed by H/He. We find that values of T_{int} from 85-105 K are realistic for the current intrinsic heat flux of the planet. For comparison, the T_{int} for our solar system’s giant planets are 99 K for Jupiter, 77 K for Saturn, 53 K for Neptune, and < 35 K (1σ upper limit) for Uranus (Pearl & Conrath 1991). The T_{int} for HD 209458b may be as high as 300 K, in order to match the planet’s current radius (Guillot & Showman 2002; Baraffe et al. 2003).

3.3. Comparative Interior Structure

Figure 7 shows the interior density distribution as a function of normalized radius for our two interior models compared these interior models of Saturn (Guillot 1999) and Neptune (Podolak et al. 1995). The Saturn and Neptune models both have two-layer cores of rock overlaid by ice. The ratio of ice to rock in these cores is based more on cosmogonical arguments than on physical evidence. The interior structure of HD 149026b may be a hybrid of the ice giants and gas giants. Uranus and Neptune are $\sim 90\%$ heavy elements, while Saturn is $\sim 25\%$ and Jupiter $\lesssim 10\%$ (Saumon & Guillot 2004). Although HD 149026b is more massive than Saturn, it has a bulk percentage of heavy elements (60-70%) more similar to that of the solar system’s ice giants.

We find that the central pressure for the model planet with the ice core 72 Mbar, while with the rock core it is 240 Mbar. At the bottom of the H/He envelope the pressure is 5.6 Mbar in the model with an ice core and 16 Mbar in the model with a rock core. Under these conditions, hydrogen is expected to be compressed into a liquid metallic state. The possibility of a relatively thin liquid metallic hydrogen layer overlying a deeper region of fluid ionic ices could lead to an interesting new regime of planetary magnetic fields. Convecting fluid ices overlying non-convective regions may be responsible for the complex magnetic fields of Uranus and Neptune (Podolak et al. 1991; Hubbard et al. 1995;

Stanley & Bloxham 2004). The convective-region geometry of a planet’s interior may well be an important factor in determining the morphology of a planet’s magnetic field (Stanley & Bloxham 2004).

3.4. Composition and the Radii of Pegasi Planets

Guillot & Gladman (2000) point out that for Pegasi planets in general, the orbital velocity of ~ 150 km/s is much larger than the planet’s escape velocity of ~ 50 km/s, meaning the planet will be inefficient at removing planetesimals near its orbit at very young ages. This is not true for Jupiter, which at its current mass and location is efficient at removing planetesimals from the solar system. Thus, Pegasi planets may accumulate more heavy elements than has been previously appreciated (Guillot 2005). HD 149026b may be towards the high-accumulation end of a continuum for Pegasi planets, possibly due to the high metallicity in the stellar system it occupies.

This leads us to consider the bulk content of heavy elements of the other transiting planets. HD 209458b is the only known transiting planet with a large radius that is difficult to model. This has suggested to many that this *one* planet harbors an additional energy source that slows its contraction (Bodenheimer et al. 2001; Guillot & Showman 2002; Baraffe et al. 2003; Winn & Holman 2005). The discovery of HD 149026b suggests another possibility. It is conceivable that all Pegasi planets would be affected by an additional energy source (yet to be identified), resulting in large radii, but that it is partly compensated by a relatively large bulk metal content, thanks to favorable conditions for planetesimal accretion. In this perspective, HD 209458b and HD 149026b would represent extremes of the metallicity range of Pegasi planets, with relatively low metallicity for HD 209458b (large radius) and a very high metallicity for HD 149026b (small radius). Given Jupiter and Saturn’s large bulk inventory of heavy elements (as much as 6 times and 14 times solar, respectively, Saumon & Guillot 2004) and the fact that most calculations on the radii of transiting planets have assumed metallicities lower than that of Jupiter (e.g. Chabrier et al. 2004; Burrows et al. 2004; Guillot 2005), this scenario is quite plausible.⁶ A similar argument was made by Guillot (2005). In tentative support of this picture, Fortney et al. (2005) found that the match to the Charbonneau et al. (2005) *Spitzer* photometry for the transiting planet TrES-1 improved as the metallicity of the model atmosphere was increased.

4. CONCLUSIONS

We have investigated aspects of the atmosphere, interior, and evolution of the new transiting planet HD 149026b. If the determination of the planet’s radius withstands additional scrutiny then this planet is unlike any other found to date. We confirm that HD 149026b is a Pegasi planet composed of 60-70% heavy elements. We note that if we had included the transit radius effect or (likely more importantly) equations of state for ices and rocks that included the additional thermal energy component, the planet would need to be even more enriched in heavy elements to match its current radius. Although we

⁶ Bodenheimer et al. (2003) and Laughlin et al. (2005) have computed evolution models with $40 M_{\oplus}$ cores for planets more massive than $1 M_J$.

calculated models with up to ten times the solar metallicity, the possibility exists that the atmosphere could be even more enriched in heavy elements. For example, the atmospheres of Uranus and Neptune are enriched in carbon (in the form of CH_4) by factors of ~ 30 over the solar value (Gautier & Owen 1989). If the planet was able to accrete significant amounts of planetesimals into its proto-atmosphere in this metal-rich environment, it could contain more heavy elements in its H/He envelope and less in its core than we have presumed, although the effects on the radius would be similar. A signature of this history would be an extremely metal-rich atmosphere.

Detection with *Spitzer* may prove challenging, given that the planet-to-star flux density ratios we predict here are $\sim 1/4$ to $1/2$ smaller than for TrES-1, given “ 4π ” reradiation for both planets. However, the $8.0\ \mu\text{m}$ flux observed from TrES-1 is larger than our models predict, and if this is also the case for HD 209458b then the case for observing HD 149026b will be strengthened. The atmosphere of HD 149026b is likely to be highly enriched in

heavy elements, in which case it would have a stratosphere that may be detected by its strong emission from 4 to $10\ \mu\text{m}$. While the star HD 209458 has a solar metallicity (Mazeh et al. 2000), its transiting planet may nevertheless have a stratosphere. Because it is bright and that it has the most favorable planet-to-star flux ratios of the known transiting planets, it is also a promising target to search for an extrasolar stratosphere. As every object in our solar system with an appreciable atmosphere exhibits a hot stratosphere, save possibly Venus, finding a stratosphere on some or all Pegasi planets would be an exciting new area of comparative planetary atmospheres.

We thank Greg Laughlin for sharing data in advance of publication and David Charbonneau for discussions about the IRAC detectors. We acknowledge support from an NRC postdoctoral fellowship (J. J. F.), NASA grants NAG2-6007 and NAG5-8919 (M. S. M.), and NSF grant AST-0406963 (K. L.). This work was supported in part by the US Department of Energy under contract W-7405-ENG-36.

REFERENCES

- Ackerman, A. S. & Marley, M. S. 2001, *ApJ*, 556, 872
 Baraffe, I., Chabrier, G., Barman, T. S., Allard, F., & Hauschildt, P. H. 2003, *A&A*, 402, 701
 Barman, T. S., Hauschildt, P. H., & Allard, F. 2005, *ApJ*, in press (astro-ph/0507136)
 Bodenheimer, P., Laughlin, G., & Lin, D. N. C. 2003, *ApJ*, 592, 555
 Bodenheimer, P., Lin, D. N. C., & Mardling, R. A. 2001, *ApJ*, 548, 466
 Burrows, A., Hubeny, I., Hubbard, W. B., Sudarsky, D., & Fortney, J. J. 2004, *ApJ*, 610, L53
 Burrows, A., Hubeny, I., & Sudarsky, D. 2005, *ApJ*, 625, L135
 Burrows, A., Marley, M., Hubbard, W. B., Lunine, J. I., Guillot, T., Saumon, D., Freedman, R., Sudarsky, D., & Sharp, C. 1997, *ApJ*, 491, 856
 Burrows, A., Marley, M. S., & Sharp, C. M. 2000, *ApJ*, 531, 438
 Burrows, A., Sudarsky, D., & Hubbard, W. B. 2003, *ApJ*, 594, 545
 Chabrier, G., Barman, T., Baraffe, I., Allard, F., & Hauschildt, P. H. 2004, *ApJ*, 603, L53
 Charbonneau, D., Allen, L. E., Megeath, S. T., Torres, G., Alonso, R., Brown, T. M., Gilliland, R. L., Latham, D. W., Mandushev, G., O’Donovan, F. T., & Sozzetti, A. 2005, *ApJ*, 626, 523
 Cooper, C. S. & Showman, A. P. 2005, *ApJL*, in press (astro-ph/0502476)
 Deming, D., Seager, S., Richardson, L. J., & Harrington, J. 2005, *Nature*, 434, 740
 Fegley, B. J. & Lodders, K. 1994, *Icarus*, 110, 117
 Fischer, D. A. & Valenti, J. 2005, *ApJ*, 622, 1102
 Fortney, J. J. & Hubbard, W. B. 2003, *Icarus*, 164, 228
 —. 2004, *ApJ*, 608, 1039
 Fortney, J. J., Marley, M. S., Lodders, K., Saumon, D., & Freedman, R. 2005, *ApJ*, 627, L69
 Fortney, J. J., Sudarsky, D., Hubeny, I., Cooper, C. S., Hubbard, W. B., Burrows, A., & Lunine, J. I. 2003, *ApJ*, 589, 615
 Gautier, D. & Owen, T. 1989, in *Origin and Evolution of Planetary and Satellite Atmospheres*, ed. S. K. Ateya, J. B. Pollack, & M. S. Matthews (Tucson: Univ. of Arizona Press), 487–512
 Gonzalez, G. 1997, *MNRAS*, 285, 403
 Guillot, T. 1999, *Planet. Space Sci.*, 47, 1183
 —. 2005, *Annual Review of Earth and Planetary Sciences*, 33, 493
 Guillot, T., Burrows, A., Hubbard, W. B., Lunine, J. I., & Saumon, D. 1996, *ApJ*, 459, L35
 Guillot, T. & Gladman, B. 2000, in *ASP Conf. Ser. 219: Disks, Planetesimals, and Planets*, ed. F. Garzon, C. Eiroa, D. de Winter, & T. J. Mahoney (San Francisco: ASP), 475
 Guillot, T. & Showman, A. P. 2002, *A&A*, 385, 156
 Hubbard, W. B. 1977, *Icarus*, 30, 305
 —. 1978, *Icarus*, 35, 177
 Hubbard, W. B., Fortney, J. J., Lunine, J. I., Burrows, A., Sudarsky, D., & Pinto, P. 2001, *ApJ*, 560, 413
 Hubbard, W. B. & Macfarlane, J. J. 1980, *J. Geophys. Res.*, 85, 225
 Hubbard, W. B. & Marley, M. S. 1989, *Icarus*, 78, 102
 Hubbard, W. B., Podolak, M., & Stevenson, D. J. 1995, in *Neptune and Triton*, ed. D. P. Cruikshank (Tucson: Univ. of Arizona Press), 109–140
 Hubeny, I., Burrows, A., & Sudarsky, D. 2003, *ApJ*, 594, 1011
 Kurucz, R. 1993, CD-ROM 13, ATLAS9 Stellar Atmosphere Programs and 2 km/s Grid (Cambridge:SAO)
 Laughlin, G., Wolf, A., Vanmunster, T., Bodenheimer, P., Fischer, D., Marcy, G., Butler, P., & Vogt, S. 2005, *ApJ*, 621, 1072
 Lodders, K. 2002, *ApJ*, 577, 974
 —. 2003, *ApJ*, 591, 1220
 Lodders, K. & Fegley, B. 2002, *Icarus*, 155, 393
 —. 2005, submitted to *Astrophysics Update*
 Marley, M. S. 1998, in *ASP Conf. Ser. 134, Brown Dwarfs and Extrasolar Planets*, ed. R. Rebolo, E. L. Martin, & M. R. Zapatero Osorio (San Francisco: ASP), 383
 Marley, M. S. & McKay, C. P. 1999, *Icarus*, 138, 268
 Marley, M. S., Saumon, D., Guillot, T., Freedman, R. S., Hubbard, W. B., Burrows, A., & Lunine, J. I. 1996, *Science*, 272, 1919
 Marley, M. S., Seager, S., Saumon, D., Lodders, K., Ackerman, A. S., Freedman, R. S., & Fan, X. 2002, *ApJ*, 568, 335
 Mazeh, T., Naef, D., Torres, G., Latham, D. W., Mayor, M., Beuzit, J., Brown, T. M., Buchhave, L., Burnet, M., Carney, B. W., Charbonneau, D., Druker, G. A., Laird, J. B., Pepe, F., Perrier, C., Queloz, D., Santos, N. C., Sivan, J., Udry, S., & Zucker, S. 2000, *ApJ*, 532, L55
 McKay, C. P., Pollack, J. B., & Courtin, R. 1989, *Icarus*, 80, 23
 Pearl, J. C. & Conrath, B. J. 1991, *J. Geophys. Res.*, 96, 18921
 Podolak, M., Hubbard, W. B., & Stevenson, D. J. 1991, in *Uranus*, ed. J. T. Bergstralh, E. D. Miner, & M. S. Matthews (Tucson: Univ. of Arizona Press), 29–61
 Podolak, M., Weizman, A., & Marley, M. 1995, *Planet. Space Sci.*, 43, 1517
 Pont, F., Bouchy, F., Queloz, D., Santos, N. C., Melo, C., Mayor, M., & Udry, S. 2004, *A&A*, 426, L15
 Santos, N. C., Israelian, G., & Mayor, M. 2004, *A&A*, 415, 1153
 Sato, B., Fischer, D. A., Henry, G. W., Laughlin, G., Butler, R. P., Marcy, G. W., Vogt, S. S., Bodenheimer, P., Ida, S., Toyota, E., Wolf, A., Valenti, J. A., Boyd, L. J., Johnson, J. A., Wright, J. T., Ammons, M., Robinson, S., Strader, J., McCarthy, C., Tah, K. L., & Minititi, D. 2005, *ApJ*, in press (astro-ph/0507009)
 Saumon, D., Chabrier, G., & van Horn, H. M. 1995, *ApJS*, 99, 713
 Saumon, D. & Guillot, T. 2004, *ApJ*, 609, 1170
 Saumon, D., Hubbard, W. B., Chabrier, G., & van Horn, H. M. 1992, *ApJ*, 391, 827
 Seager, S., Richardson, L. J., Hansen, B. M. S., Menou, K., Y-K. Cho, J., & Deming, D. 2005, *ApJ*, submitted (astro-ph/0504212)
 Stanley, S. & Bloxham, J. 2004, *Nature*, 428, 151
 Thompson, S. L. 1990, ANEOS—Analytic Equations of State for Shock Physics Codes, Sandia Natl. Lab. Doc. SAND89-2951
 Toon, O. B., McKay, C. P., Ackerman, T. P., & Santhanam, K. 1989, *J. Geophys. Res.*, 94, 16287
 Winn, J. N. & Holman, M. J. 2005, *ApJL*, submitted (astro-ph/0506468)
 Zharkov, V. N. & Trubitsyn, V. P. 1978, *Physics of planetary interiors (Astronomy and Astrophysics Series, Tucson: Pachart, 1978)*

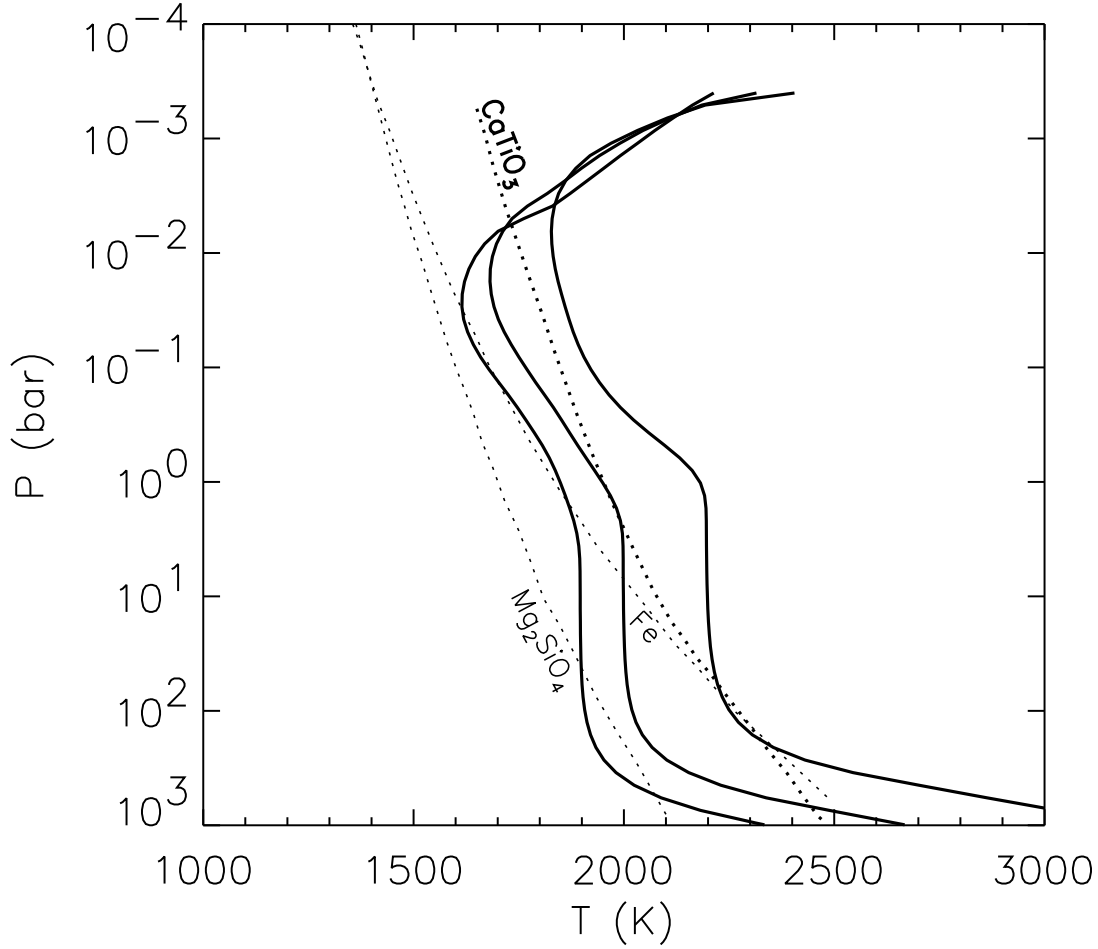


FIG. 1.— Cloud-free atmospheric P - T profiles for $[M/H]=0, 0.5,$ and 1 (from left to right at depth). These profiles include the opacity of TiO and VO at low pressure, which is not realistic for some profiles, as the profiles cross the CaTiO_3 condensation curve near 1 kbar ($[M/H]=0$ and 0.5) and potentially near 100 bar for the case with $[M/H]=1$. Condensation curves are from Lodders & Fegley (2005).

TABLE 1
MODEL PLANET-TO-STAR FLUX DENSITY RATIOS IN *Spitzer* BANDS FOR HD 149026B

Model	T_{eff} (K)	$3.6 \mu\text{m}$	$4.5 \mu\text{m}$	$5.8 \mu\text{m}$	$8.0 \mu\text{m}$	$24 \mu\text{m}$
$3\times, 4\pi$	1736	0.24	0.30	0.37	0.45	0.68
$3\times, 4\pi$, no clouds	1734	0.24	0.28	0.35	0.44	0.66
$3\times, 2\pi$	2148	0.43	0.60	0.71	0.85	1.11
$10\times, 4\pi$	2025	0.37	0.55	0.66	0.82	1.09

Note. — All ratios have been multiplied by 1000. Abundances and number of steradians for reradiation are given.

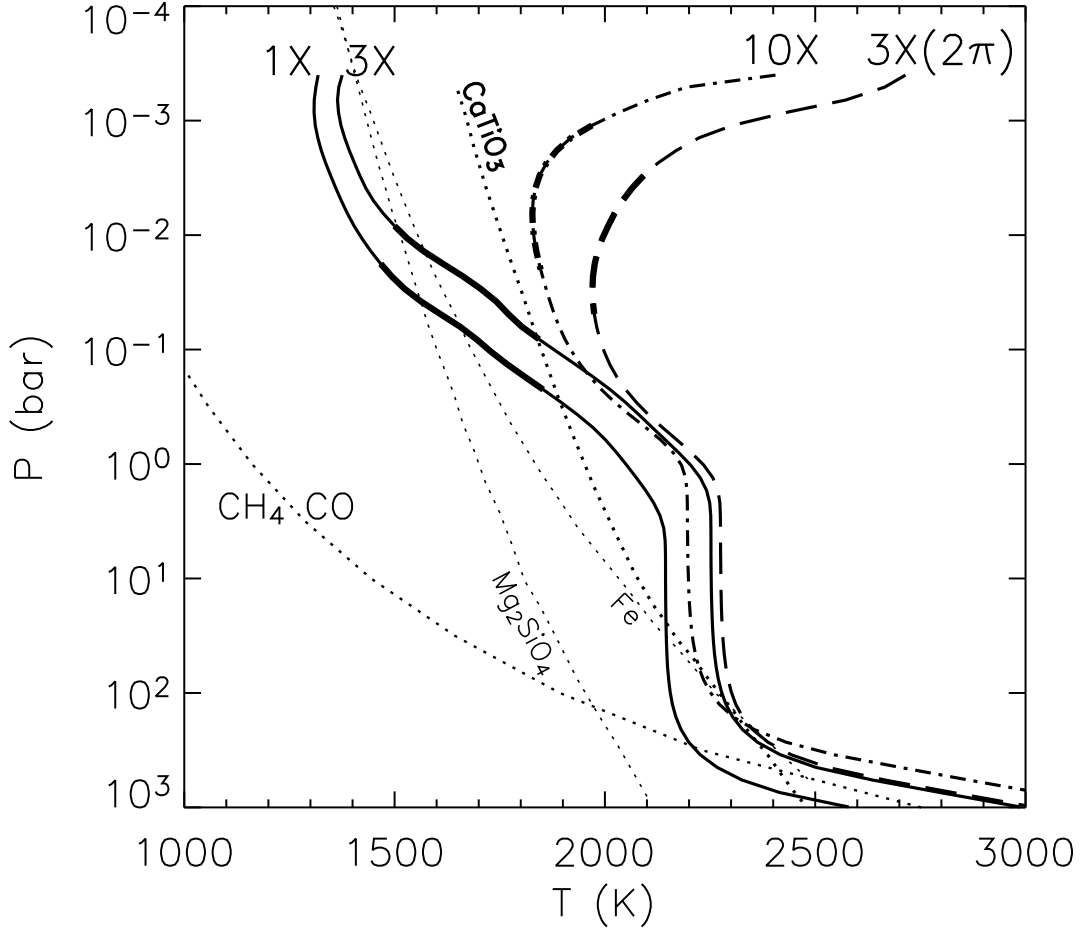


FIG. 2.— Atmospheric P - T profiles for $[M/H]=0, 0.5$ and 1 (1X, 3X, and 10X, respectively). In the models with $[M/H]=0$ and 0.5 , the opacity of TiO and VO has been removed at pressures less than 10 bar, but the opacity of clouds of forsterite and iron is included. The $[M/H]=1$ model may not cross the CaTiO_3 condensation curve, depending on the exact value of T_{int} so TiO has been retained in the upper atmosphere. The “3X(2π)” model, which assumes that the absorbed stellar flux can only be reradiated on the planet’s day side, is everywhere hotter than the CaTiO_3 condensation curve. The thick part of each profile shows the extent of the brightness temperatures for each model in the 3 to 30 μm wavelength range. Also shown is the curve where the abundances of CH_4 and CO are equal, for solar composition.

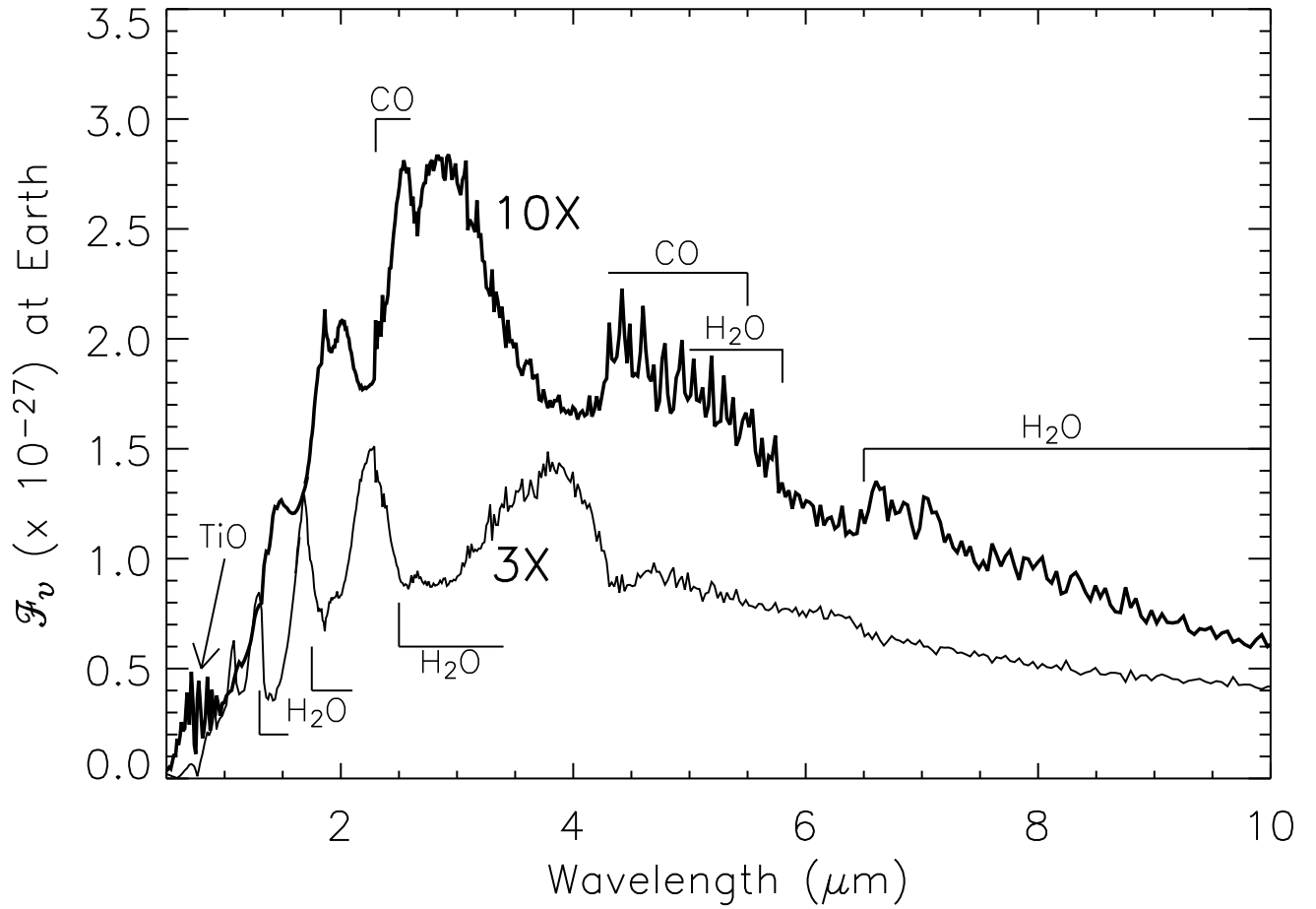


FIG. 3.— Infrared spectra of the $[M/H]=0.5$ (thin line) and 1 (heavy line). The flux is in 10^{-27} $\text{erg s}^{-1} \text{cm}^{-2} \text{Hz}^{-1}$. Many features seen in absorption in the $[M/H]=0.5$ model can be seen in emission in the $[M/H]=1$ model. Most prominent are the H₂O and CO features in the infrared. TiO can be seen in emission in the optical in the $[M/H]=1$ model, whereas the $[M/H]=0.5$ model has strong absorption due to Na and K in the optical.

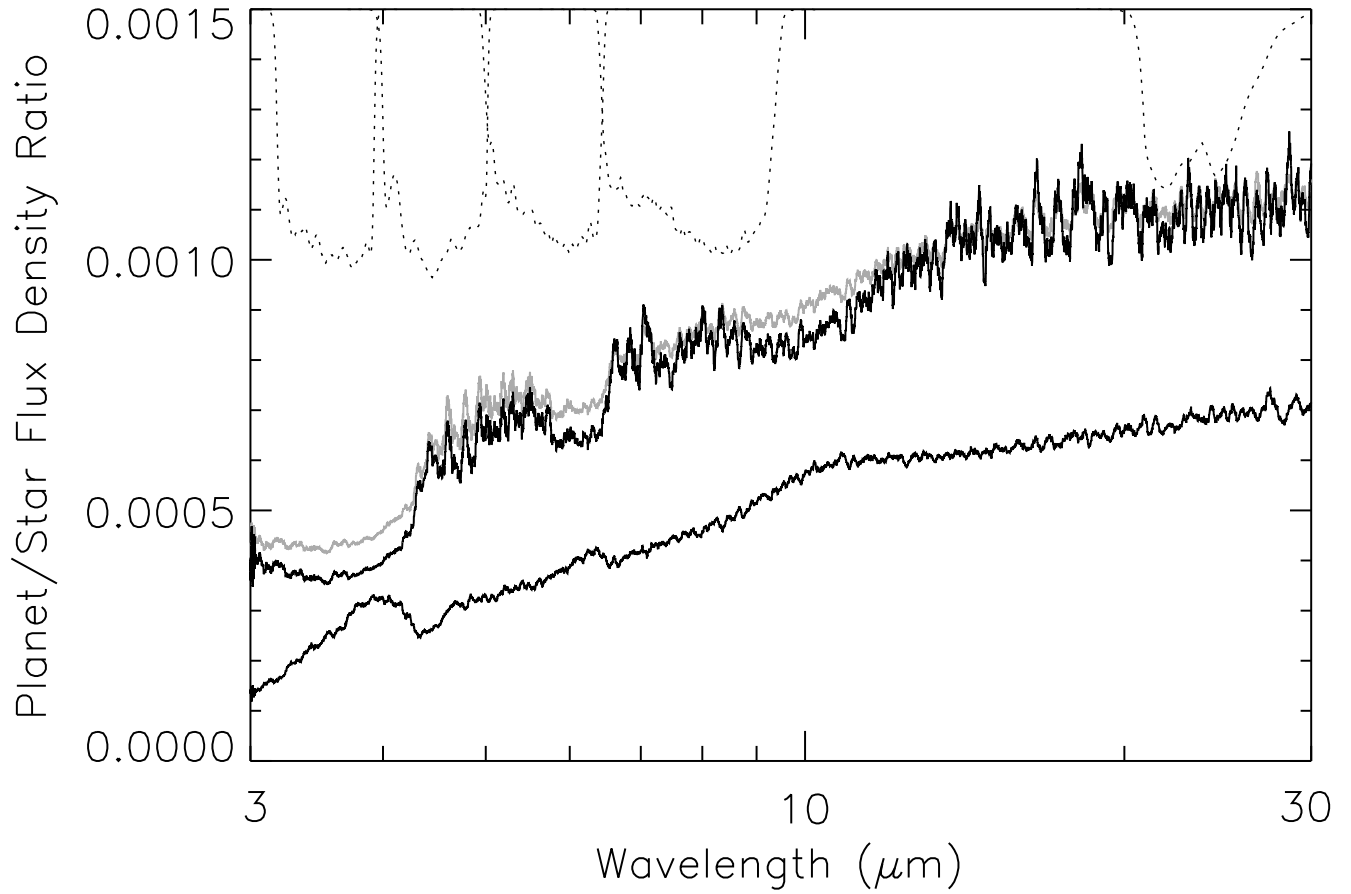


FIG. 4.— Planet-to-star flux density ratios for three planet models. The lower black curve is the cloudy model with $[M/H]=0.5$. The upper black curve is the $[M/H]=1$ model. The grey curve is the model with $[M/H]=0.5$ and 2π steradian reradiation. Shown in dotted lines, hanging from above, are the sensitivity functions of the 4 IRAC bands and the MIPS $24\ \mu\text{m}$ band.

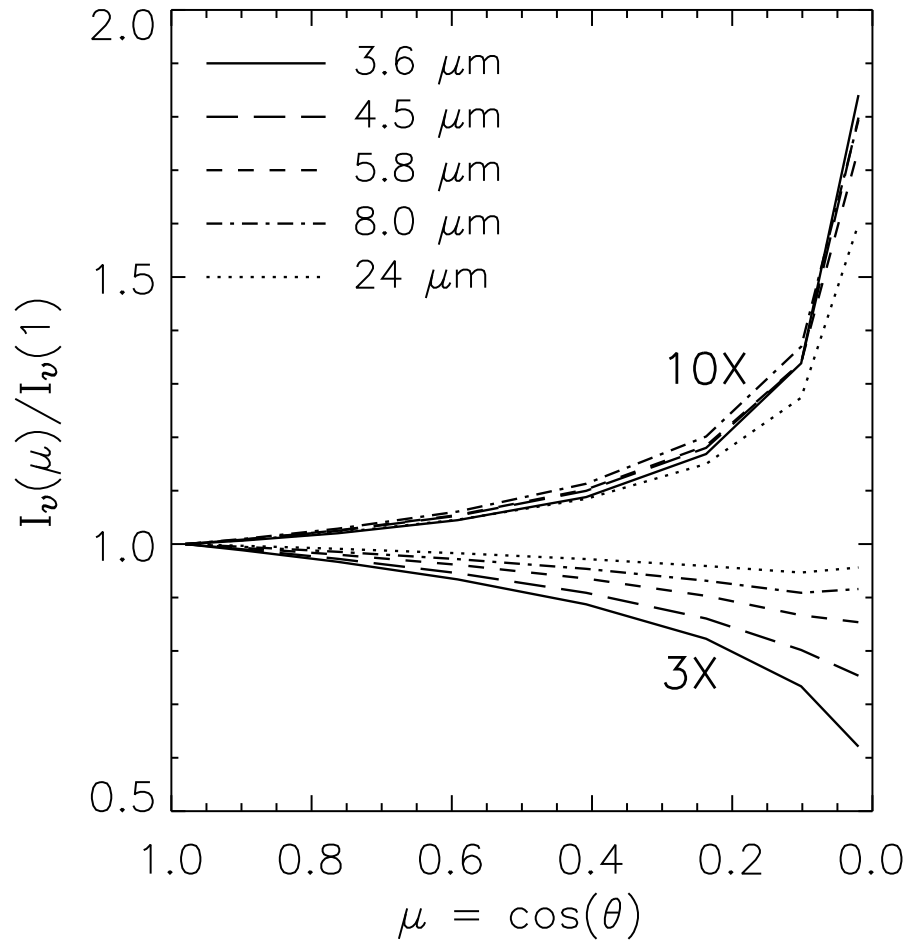


FIG. 5.— Limb darkening profile for two atmosphere models in 5 different *Spitzer* bandpasses. The “10X” curves are for the $[M/H]=1$ atmosphere models with a hot stratosphere. The “3X” curves are for the cloudy, $[M/H]=0.5$ atmosphere models. (See Figure 2.)

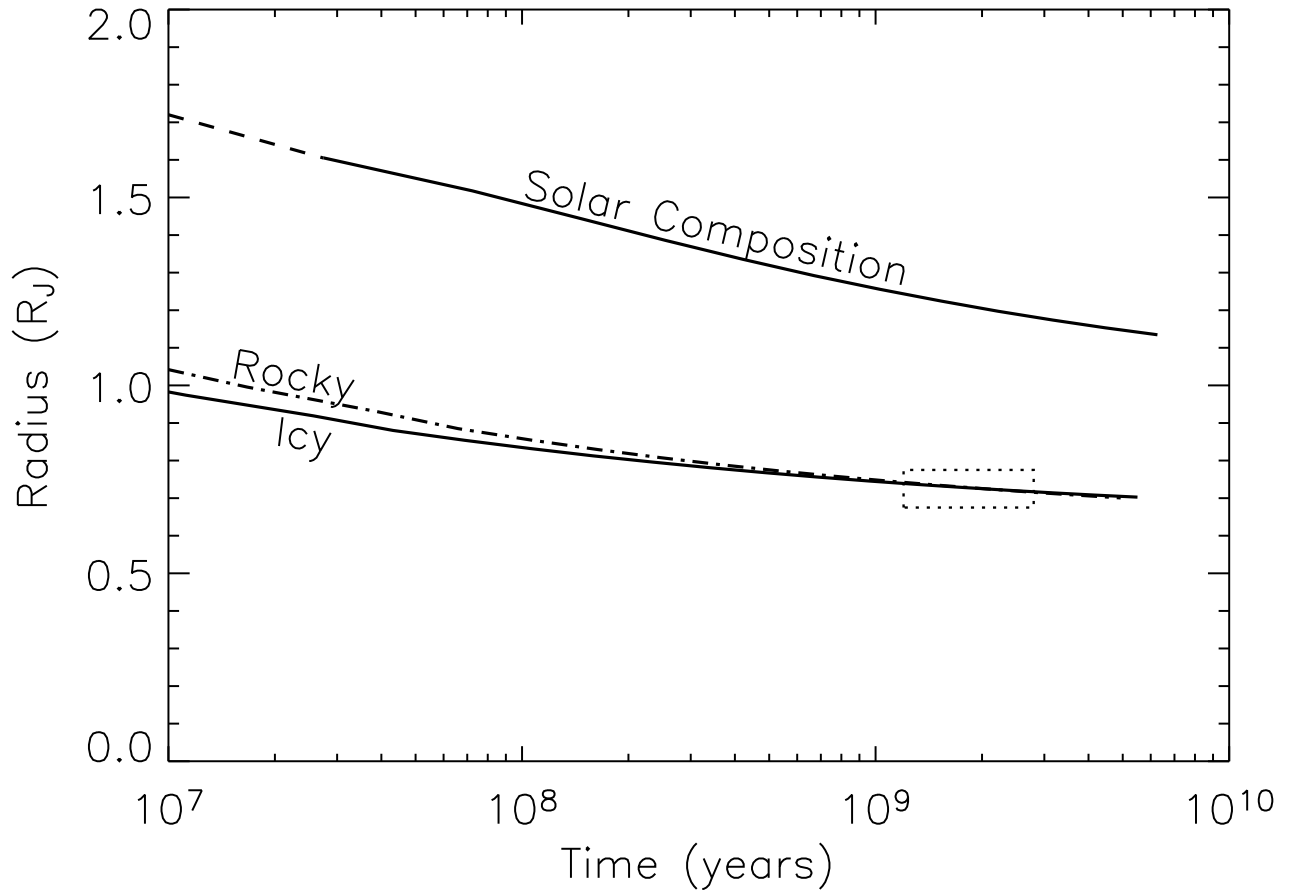


FIG. 6.— Radii of HD 149026b planet models. A planet model of solar composition is shown for comparison purposes. The two models that match the observed radius at 2 Gyr include a H/He envelope with $Z=0.045$, approximately 3 times the solar metallicity, which matches the atmosphere model. The “Rocky” model includes a core of $65.5 M_{\oplus}$ of olivine, while the “Icy” model includes a core of $77 M_{\oplus}$ of ice. The age/radius error box is from Sato et al. (2005). The dashed portion of the solar composition model indicates where the planet was off the atmosphere grid due to low gravity.

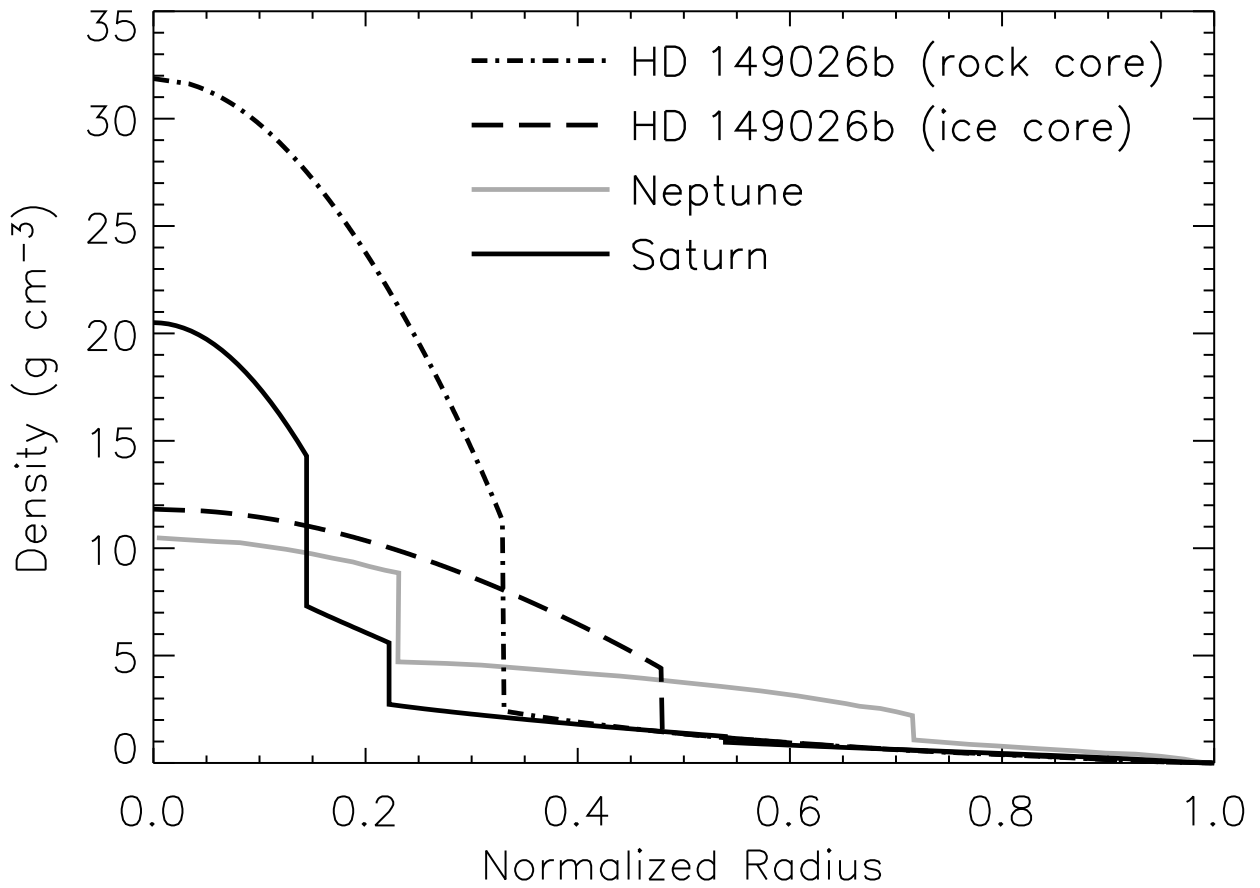


FIG. 7.— Interior density profiles of two possible models for HD 149026b compared with Neptune and Saturn. The Neptune profile is from Podolak et al. (1995) and the Saturn profile is from Guillot (1999). The Saturn and Neptune models have a layer of ice overlying a central rocky core. The two profiles of HD 149026b assume that $[M/H]=0.5$ in the H/He envelope and a core made entirely of either ice or rock.